AIRBORNE POLLEN OBSERVED BY POLLY^{XT} RAMAN LIDAR AT FINOKALIA, CRETE

Xiaoxia Shang[1,*], Stephanie Bohlmann[1], Maria Filioglou[1], Elina Giannakaki[1,2], Mikko R.A. Pitkänen[1], Annika Saarto[3], Vassilis Amiridis[4], Maria Kanakidou[5], Mika Komppula[1]

[1]Finnish Meteorological Institute, P.O. Box 1627, 70211 Kuopio, Finland
[2]Department of Environmental Physics and Meteorology, University of Athens, 15784 Athens, Greece
[3]Biodiversity Unit, University of Turku, 20014 Turku, Finland
[4]IAASARS, National Observatory of Athens, 15236 Athens, Greece
[5]ECPL, Department of Chemistry, University of Crete, 70013 Heraklion, Greece
**Email: xiaoxia.shang@fmi.fi*

ABSTRACT

In order to document and study airborne pollen in the Mediterranean region, a pollen measurement campaign was performed during February-May 2018, at the Finokalia station in Crete. A ground-based multi-wavelength Raman polarization lidar Polly^{XT} performed continuous measurements, together with a Hirst-type Burkard pollen sampler. The optical properties of pollen layers with presence of airborne pollen are retrieved and presented. Dust-free condition is applied for pollen study, using the dust models.

1. INTRODUCTION

Airborne pollen is recognized as one of the major agents of allergy-related diseases such as asthma, rhinitis, and atopic eczema. Pollen is also a form of biogenic air pollutant which affects both the solar radiation reaching the Earth and cloud optical properties [1]. Various networks are built to monitor pollen concentrations at ground level using in situ instruments [2]. One of the most allergenic tree pollen is produced by birch (*Betula*) in north, central, and Eastern Europe. In the Mediterranean region, olive (*Olea europaea*) pollen is considered as one of the most important causes of respiratory allergic disease, whereas cypress (*Cupressus*) releases an enormous amount of anemophilous pollen and has been recognized to be responsible for a large part of total annual amount of airborne pollen [3].

Recently an increasing interest in pollen has arisen in the aerosol lidar community. It has been observed that the non-spherical pollen grains generate strong depolarization [4][5]. Our previous study on pollen shows that lidar measurements can detect the presence of pollen grains in the atmosphere, and lidar derived parameters (e.g. depolarization ratio and Ångström) provide the possibility to identify different pollen types (e.g. birch and pine pollen) [6]. In order to get more information on the distribution of different pollen types in the atmosphere, Finokalia station, located at a remote coastal site in the Eastern Mediterranean Sea, was selected for the pollen campaign. Marine and dust aerosols in this area make the pollen detection and separation more challenging.

2. METHODOLOGY

2.1 Measurement site

A pollen measurement campaign was performed during February-May 2018, at the Finokalia station (35°20'N, 25°40'E) on the north coast of Crete, Greece. The Finokalia station is located at the top of a hilly elevation (238 m above sea level) facing the sea within a sector 270° to 90°. The site is ideal for studying natural aerosols such as mineral dust, marine aerosols, and airborne pollen, since it is not affected by anthropogenic emissions [7]. The nearest large urban center, to the station, is Heraklion with 150 000 inhabitants located 70 km west of Finokalia.

2.2 Instruments

The pollen concentration, for two periods between 23 February and 26 March, and 10 April to 12 May 2018, was retrieved by the Burkard 7-Day Recording Volumetric Spore Sampler [8], placed 4 meters above ground level (agl). This Hirst-type pollen sampler enables microscopical identification of pollen types and their concentration with a 2-hour time resolution.

A ground-based multi-wavelength Raman polarization lidar Polly^{XT} [9] performed continuous measurements. The lidar is equipped with three

elastic channels (355 nm, 532 nm and 1064 nm), two rotational vibrational Raman channels (387 nm and 607 nm), two linear depolarization channels (355 nm and 532 nm), and one water vapor channel at 407 nm. The combined use of near and far field telescopes provides reliable vertical profiles of aerosol optical properties from 0.25 km to 10 km agl [10].

2.3 Dust models

The island of Crete is very often affected by windblown dust originating from the Sahara, due to its proximity to the African coastline. In order to avoid the dust effects on pollen properties retrieval, only dust-free periods are considered in this study. The periods are defined using two models.

The NMMB/BSC-Dust (Non-hydrostatic Multiscale Model / Barcelona Supercomputing Center) [11] is an online multi-scale atmospheric dust model designed to accurately describe the dust cycle in the atmosphere, and intended to provide short to medium-range dust forecasts for both regional and global domains. It provides vertical profiles (from 0 to 12 km agl) of dust concentration every 6 hours, with a horizontal resolution of 0.3°×0.3°.

The second aerosol product was the Copernicus Atmosphere Monitoring Service (CAMS) near-real-time dust mass mixing ratio forecast [12][13]. The model is based on the global ECMWF-IFS NWP model, and is extended with CAMS atmospheric composition features including data assimilation from satellites and other observational data. The 3-hourly short range dust forecast data used in this study are provided at 25 pressure levels in a 0.4° regular grid.

2.4. Lidar data processing

During cloud-free day-time, the aerosol optical depth derived from the AERONET sun-photometer station of Finokalia (http://aeronet.gsfc.nasa.gov/) is used as a constraint to retrieve the altitude-independent lidar ratio (LR). The Klett method [14] is then applied to retrieve the vertical profiles of aerosol extinction coefficient and backscatter coefficient. During night-time, the standard Raman inversion algorithm is used, which provides additional LR profile [15][16]. LR is considered an important criterion to analyse atmospheric aerosols, as it depends on their single scattering albedo and backscatter phase function, and is thus a function of size distribution and chemical composition.

The volumetric depolarization ratio (VDR) and linear particle depolarization ratio (PDR) at 355 nm and 532 nm are retrieved [17]. The PDR provides information on the shape of the scattering particles. Multi-wavelength measurements allow the retrieval of Ångström exponents (Å), which is related to the particle nature, mostly the size.

A temporal averaging of 2 hours is used to increase the signal-to-noise ratio and to match the Hirst-type pollen sampler data.

3. RESULTS

3.1 Airborne pollen

During the campaign, 30 types of pollen were measured by Burkard Sampler. The five most abundant airborne pollen types were: *Olea* (Olive), *Cupressus* (Cypress), *Platanus* (plane trees), *Quercus* (Oak), and *Ulmus* (Elm), their microphotographs are shown in Figure 1. Their shapes are almost spherical, with size ranging from ~15 to ~30 μm. Sensitisation rates to olive and cypress pollen in Greece are 31.8% and 12.7%, compared to 8.2% to plane pollen and 7.6% to oak pollen. Elm pollen appears in the air in fairly small quantities [18]. The pollination periods for several pollen types were often overlapped, thus a mixture of pollen types were always observed in the atmosphere.

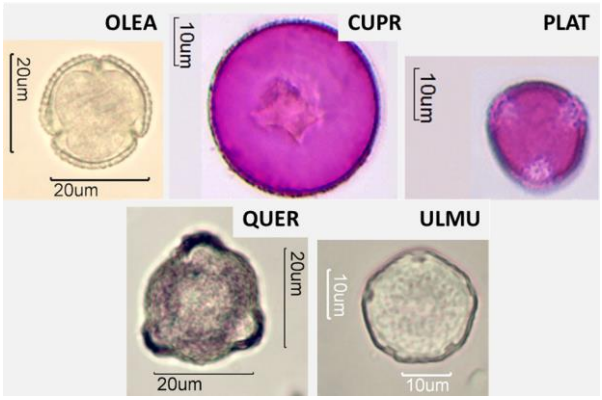

*Figure 1. Microphotographs of pollen grains: **Olea** (Olive), **Cupr**essus (Cypress), **Plat**anus (plane tree), **Quer**cus (Oak), **Ulmu**s (Elm). Source: http://www.microlabgallery.com/ and https://pollen.tstebler.ch/.*

3.2 Aerosol optical properties

A "pollen layer" is defined as the lowest observed layer; we assume that pollen grains are distributed in this layer, and that anthropogenic emissions were not present. "Clean atmosphere" and "non-typed aerosols" were removed from our analysis following the criteria of aerosol typing given in [19]. The top heights of pollen layers during the campaign ranged from 0.4 to 3 km agl. Mean values of the optical properties in the pollen layer within 2 hours were used.

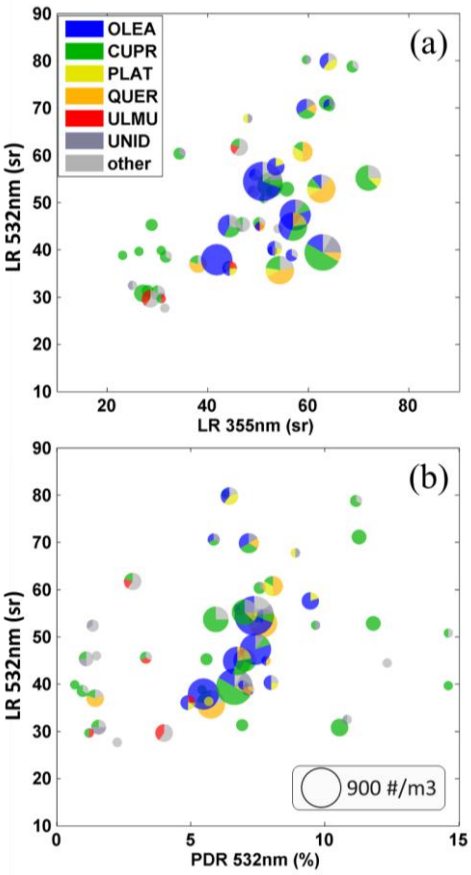

Figure 2. (a) Lidar ratio (LR) at 355 nm, and (b) linear particle depolarization ratio (PDR) against LR at 532 nm for night-time measurements. Mean values within 2 hours in the defined "pollen layer" are used. The size of the symbols is relative to the total pollen concentration measured by the Burkard sampler, the main pollen types are shown by colors, UNID means unidentified pollen.

3.2.1 Night-time observations

Night observations were obtained and analyzed during the period. Mean values in the pollen layers of (a) LR at 355 nm, and (b) PDR at 532 nm against LR at 532 nm are shown in Figure 2. LR in both wavelengths ranged between 20 and 80 sr, with a mean value of 47.1 ±13.0 sr at 355 nm and 48.1 ±13.9 sr at 532 nm. Unlike our previous study of pine pollen in Finland with high depolarization, the maximum PDR was found to be ~15%, with a mean value of 6.5 ±3.5%. This indicates that pollen observed during our campaign in this Mediterranean area are almost spherical. The backscatter-related Ångström exponent (Å) at 355/532 nm is 1.0 ±0.4, which indicates relatively small pollen particles.

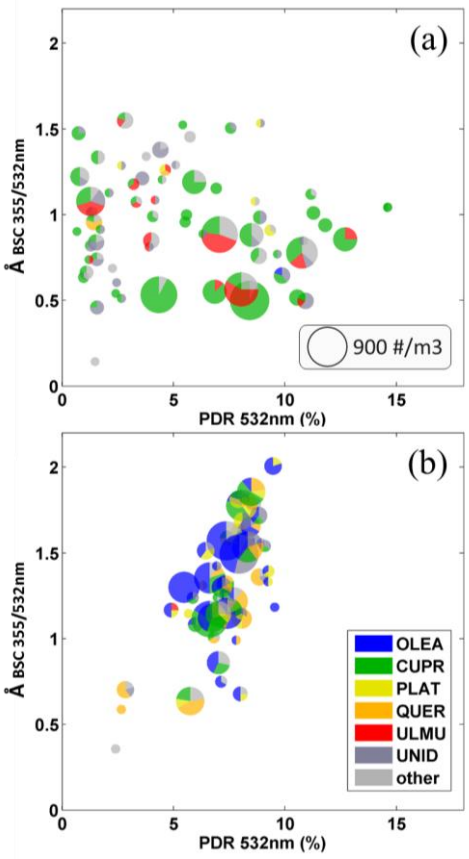

Figure 3. Lidar-derived linear particle depolarization ratio (PDR) at 532 nm against backscatter-related Ångström exponents (355 nm/532 nm), for the periods of (a) 23 Feb to 26 Mar., and (b) 10 Apr. to 12 May, 2018. Mean values within 2 hours in the defined "pollen layer" are used. Legend is same as in Figure 2.

3.2.2 All-day observations.

The cypress tree shed profuse amounts of pollen 6-7 months of the year. *Cupressus* is observed for the whole campaign, with the highest pollination period at the beginning of March. Olive flowers

from mid spring to early summer. *Olea* pollen was observed from April to May in this campaign, with highest pollination period at the end of April. Two periods are considered separately in this study: (i) 23 Feb. to 26 Mar. 2018, *Cupressus* is the dominant pollen; (ii) 10 Apr. to 12 May. 2018, *Olea* is dominant. Mean values in the pollen layers of the backscatter-related Ångström exponent (Å) at 355 / 532nm and PDR at 532 m are shown in Figure 3. For the period (i), PDR values for the pollen layers range from very small to about 15%, with a mean value of 5.6 ±3.9%. The Å is found to be 1.0 ±0.3. For the period (ii), PDR values are more concentrated at 7.3 ±1.6%, and Å is bigger compared to the period (i), with the mean value of 1.3 ±0.4. The smaller Å of period (i) is related to the bigger size of the dominate pollen grain (*Cupressus*). With these retrieved values of optical properties, the conventional classification algorithms will always identify these particle as marine mixtures, pollution mixtures, or dust mixtures [20].

CONCLUSION

We characterized the optical properties of airborne pollen in a remotely located site in the Mediterranean region, using a multi-wavelength Raman polarization lidar and a Hirst-type Burkard pollen sampler. We found that the linear particle depolarization ratio of pollen layer was relatively small, with a maximum value of ~15%, since the shape of the majority of pollen types in this region is quasi-spherical. Optical properties of airborne pollen retrieved in this study are classified as "mixture" using conventional classification algorithms in literature. Future work will be focused on the aerosol separation of dust, pollen and marine aerosols.

ACKNOWLEDGEMENTS

This work was supported by the Academy of Finland (project no. 310312). The authors would like to thank the AERONET network for sun-photometer products. Dust data used in this study is from the NMMB/BSC-Dust model, operated by the Barcelona Supercomputing Center (http://www.bsc.es/ess/bsc-dust-daily-forecast/), or generated using Copernicus Atmosphere Monitoring Service Information (2019).

REFERENCES

[1] A. L. Steiner, et al., Geophys. Res. Lett., 42, 3596–3602 (2015)
[2] T. Giesecke, et al., Veg. Hist. Archaeobot., 19, 247–258 (2010)
[3] G. D'Amato, et al., Allergy, 62 (9), 976-990 (2007)
[4] M.Y. Noh, et al., Atmos. Environ., 69, 139-147 (2013)
[5] M. Sicard et al., Atmos. Chem. Phys., 16, 6805-6821 (2016)
[6] X. Shang, et al., in Proceedings of European LiDAR Conference (ELC), (2018)
[7] S. Apostolopoulou, et al., in Proceedings of the 27th International Laser and Radar conference (ILRC27), (2017)
[8] J. M. Hirst, Ann. Appl. Biol., 39, 257-265 (1952)
[9] R. Engelmann, et al., Atmos. Meas. Tech., 9, 1767–1784 (2016)
[10] S. Solomos, et al., Atmosphere, 9, 240 (2018)
[11] C. Pérez, et al., Atmos. Chem. Phys., 11, 13001-13027 (2011)
[12] Up-to-date online documentation of the global CAMS-IFS forecasts https://atmosphere.copernicus.eu/global-production-system (valid on 2019-03-22)
[13] Quarterly quality assurance documents of the CAMS-IFS atmospheric composition forecasts https://atmosphere.copernicus.eu/node/325 (valid on 2019-03-22)
[14] J. D. Klett, Appl. Optics, 20, 211–220 (1981)
[15] A. Ansmann, et al. Opt. Lett., 15, 746 (1990)
[16] X. Shang, et al., Atmos. Meas. Tech., 11, 6525-6538 (2018)
[17] P. Chazette, et al., Atmos. Chem. Phys., 12, 7059–7072 (2012)
[18] D. Gioulekas, et al., Allergy, 59: 174–184. (2004)
[19] H. Baars, et al., Atmos. Meas. Tech., 10, 3175–3201 (2017)
[20] B. Heese, et al., Atmos. Chem. Phys., 17, 6679-6691 (2017)